DOI:
10.1002/jrs.5576

Document Version
Early version, also known as pre-print

3-color coherent anti-Stokes Raman scattering with optical non-resonant background removal

Brad Littleton, Priyank Shah, Thomas Kavanagh, and David Richards*

Department of Physics, King's College London, London, WC2R 2LS, United Kingdom

E-mail: david.r.richards@kcl.ac.uk

Abstract

Broadband coherent anti-Stokes Raman scattering (B-CARS), excited through intra-pulse 3-color processes in which both the pump and Stokes photons are derived from a broadband beam, enables diffraction-limited hyperspectral Raman imaging over the entire fingerprint spectral region with a speed and sensitivity far superior to that possible with conventional spontaneous Raman confocal micro-spectroscopy. We extend the theory of spectral interferometric polarization coherent anti-Stokes Raman scattering (SIP-CARS) to include 3-color excitation processes. This allows for the B-CARS measurement of polarized Raman-equivalent spectra free of the non-resonant background, without the requirement for post-acquisition computational processing. We demonstrate the simultaneous measurement of both 3-color and 2-color SIP-CARS, at low and high Raman shifts, respectively, in good agreement with theory. These proof of concept results pave the way for photon-efficient SIP-CARS signal generation with ultrafast lasers, for all-optical, fast, quantitative Raman hyperspectral imaging.

Introduction

Coherent anti-Stokes Raman scattering (CARS) is a four-wave mixing (FWM) process enhanced by molecular vibrational resonances, such that the signal generated is closely related to spontaneous Raman spectroscopy, but with the inherent optical sectioning of a multiphoton technique and with orders of magnitude greater signal strength. Broadband coherent anti-Stokes Raman scattering (B-CARS) allows the acquisition of an entire vibrational spectrum in a single exposure, enabling rapid Raman imaging with full spectral content for detailed chemical specificity at every point in an image.[1,2] Efficient excitation schemes based on a combination of inter-pulse (termed 2-color and most efficient in the C-H stretch region) and intra-pulse (termed 3-color and most efficient in the fingerprint region) excitation mechanisms have lowered hyperspectral acquisition times to 3.5 ms in biological tissue[3] (multispectral vibrational imaging methods based on stimulated Raman scattering[4–7] are able to achieve higher speeds, but at the expense of spectral breadth and/or detail). As with other CARS techniques, the non-resonant background (NRB) arising from the electronic material response is an issue in B-CARS, which may be removed through computational data processing.[8] Spectral interferometric polarization CARS (SIP-CARS) is a quantitative B-CARS technique that optically removes the NRB, using only passive polarization optics, and directly gives spectra equivalent to polarized spontaneous Raman measurements.[9] SIP-CARS has previously been demonstrated in a 2-color CARS modality; this paper shows its extension to 3-color and hybrid 2- and 3-color CARS spectroscopy demonstrating the potential of SIP-CARS for fast, photon-efficient hyperspectral Raman imaging, with the advantages of an all-optical implementation for direct

spectral read-out and additional information of molecular symmetry.

In CARS three input photons, termed pump, Stokes, and probe, are tightly focused onto a sample, with the resultant anti-Stokes signal photon produced via a third-order non-linear optical process, the energy level diagram for which is illustrated in Fig. 1(a). Other FWM processes, which do not involve a vibrational resonance, are also possible with the same four photons (as shown by the $\omega_p \rightarrow \omega'_{pr} \rightarrow \omega'_S \rightarrow \omega_{aS}$ sequence in Fig. 1(a)) and it is these interactions that give rise to the NRB.

For experimental simplicity, CARS is often implemented with degenerate (narrowband) pump and probe beams, meaning that the three input photons can be generated from only two lasers. This is therefore termed 2-color CARS. When performing 2-color B-CARS, a spectrally broad pulse is used as the Stokes beam to probe a wide vibrational spectral range. However, two photons of different energy from within the broadband pulse can also generate vibrational coherence, which is then probed by the narrowband laser. In this case, the input photons all have different energies, and this is termed the 3-color process.[3,10] For 3-color CARS, the vibrational coherence is effectively generated via the autocorrelation of the broadband beam, while for the 2-color process it is generated by difference frequencies arising from interaction between the narrowband and broadband beams. By spectrally separating the narrowband and broadband beams the two mechanisms can be made to simultaneously generate signal in different regions of the spectrum (3-color at lower energies and 2-color at higher energies), giving a more photon-efficient way of generating broadband CARS spectra.[3]

Spectral interferometric polarization CARS

NRB removal using passive polarization optics

The NRB is a coherent background with a fixed phase relationship to the vibrational signal; the resulting interference leads to distorted line-shapes and signals that depend non-linearly on both analyte and solvent concentration. Many methods have been developed to remove the NRB and restore the spectral line-shapes.[1] Optical methods tend to be experimentally complex or require spectral or phase scanning. Computational methods usually result in phase and amplitude errors; however, they have been shown to work well if certain conditions are met.[11–14] Spectral interferometric polarization CARS (SIP-CARS) is a simple and robust interferometric optical method which removes the NRB and restores the spectral line-shapes without the need for computational signal recovery.[9] Spectra are equivalent to polarized spontaneous Raman spectra, and are amplified by the non-resonant response, which is essential for fast acquisition.

The CARS signal intensity is determined by the squared magnitude of the third order susceptibility

$$\left|\chi^{(3)}\right|^2 = \chi_{NR}^2 + 2\chi_{NR} Re\left\{\chi_R\right\} + \left|\chi_R\right|^2 \quad (1)$$

where χ_R and χ_{NR} are components resonant and non-resonant with vibrational modes, respectively. Away from electronic resonances χ_{NR} is real, and the imaginary component of the resonant response, $Im\left\{\chi_R\right\}$, is directly related to the spontaneous Raman spectrum.[15] SIP-CARS recovers the imaginary component of the total non-linear response directly, thereby removing the NRB and real signal component, by exploiting the phase shifts that occur at the vibrational resonance, along with symmetries in the CARS polarization response.

For circularly (or elliptically) polarized light there is a fixed phase relationship between orthogonal polarization projections. Therefore, by generating CARS with elliptically polarized fields, it is possible to create a situation where the extra phase shift due to the polarization brings resonant oscillations either into or out of phase with the non-resonant response. This occurs along particular polarization directions; measuring the anti-Stokes spectrum along these polarizations gives two spectra: one with the imaginary components added to the real, and

the other with the imaginary components subtracted from the real. By taking the difference between these two spectra, the real components (including the NRB) cancel, leaving only the imaginary response. As the spectra are measured simultaneously, interferometric NRB removal is performed in a single exposure. Other real signal components, such as fluorescence, are common-mode and cancel automatically in the SIP-CARS spectrum. Because vibrational modes are being driven with specific polarization states the polarization response of the vibration, as characterized by the depolarization ratio of the mode, ρ, influences the magnitude of the response. It can be shown analytically that the SIP-CARS spectrum is equivalent to a fixed linear combination of polarized spontaneous Raman spectra (Eqn (3) below). The third-order response is solved exactly, without assumptions on the relative strength of resonant and non-resonant components.[16,17]

2-color SIP-CARS

The theory for 2-color CARS (narrowband pump and probe fields) has been described by us previously.[9] For the case of elliptical pump-probe field and linear Stokes field polarizations the 2-color SIP-CARS signal is given by

$$I_{2col} = \frac{1}{2}(1-3\rho)\sin(4\phi)\,\chi_{NR} Im\left\{\chi^R_{1111}\right\} I_{pr} I_p I_S \tag{2}$$

where the subscripts pr, p and S denote the probe, pump and Stokes fields, respectively, and ρ is the depolarization ratio of the mode ($\rho = \chi_{1221}/\chi_{1111}$). The ellipticity of the pump/probe fields is characterized by ϕ, defined as the angle between the fast axis (set parallel to the Stokes polarization) of a quarter waveplate and an input linear polarization. From Eqn (2), the SIP-CARS signal is proportional to $Im\{\chi_R\}$ and amplified by χ_{NR}. Depending on the symmetry of the mode, ρ can have values $0 < \rho < 3/4$ and hence the amplitude of I_{2col} is negative for $\rho < 1/3$. I_{2col} can be shown to be equivalent to a linear combination of parallel ($R_\parallel$) and perpendicular ($R_\perp$) polarized spontaneous Raman spectra:

$$I_{2col} \propto R_\parallel - 3R_\perp. \tag{3}$$

SIP-CARS spectra are therefore directly related to polarized spontaneous Raman measurements, as has been shown experimentally by us previously.[9]

3-color SIP-CARS

In the 3-color mechanism both pump and Stokes fields arise from the broadband laser. We will therefore distinguish the input lasers by the terms narrowband and broadband, and use the terms pump, Stokes and probe only to denote the steps in the CARS process Fig. 1(a). Following a similar procedure to the 2-color theory we begin by considering all spectrally resolved contributions (i.e. with narrowband probe) that can result from the input polarization state, Fig. 1(b). We consider the case of a linearly polarized broadband beam and elliptically polarized narrowband beam, as this is simpler to implement experimentally than accurately controlling an elliptical polarization of a broadband beam at a tight focus. The narrowband field amplitude is E_n with x- and y-components E_{n_x} and E_{n_y}, with the x-axis defined as that of the linear polarization of the broadband field, E_b. By conservation of energy, an anti-Stokes photon can only be generated if the Stokes photon comes from the broadband laser (which has longer wavelength); the pump photon, however can come from either the narrowband or broadband beam.

To perform SIP-CARS, two spectra, S_+ and S_-, are measured along the polarization directions $\mathbf{s}_+$ and $\mathbf{s}_-$ in Fig. 1(b). If P_x and P_y are the induced material polarizations parallel and orthogonal to the broadband polarization, respectively, then $S_+ \propto |P_x + P_y|^2/2$ and $S_- \propto |P_x - P_y|^2/2$, with their difference given by:[9]

$$I_{SIPCARS} = (S_+ - S_-) \propto P_x P_y^* + P_x^* P_y \tag{4}$$

The contributions to P_x and P_y can be found from the supplementary information in Camp

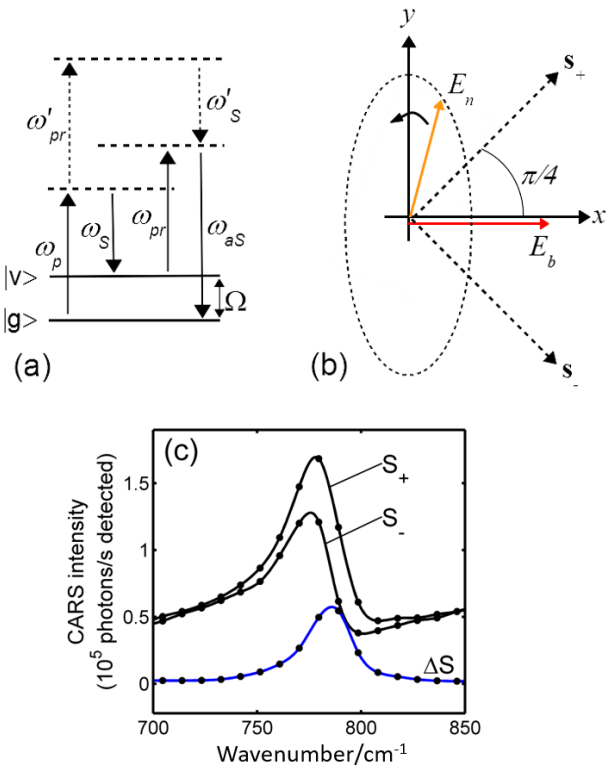

Figure 1: (a) Energy level diagram. CARS involves transitions $\omega_p \rightarrow \omega_{pr} \rightarrow \omega_S \rightarrow \omega_{aS}$; an example NRB pathway is $\omega_p \rightarrow \omega'_{pr} \rightarrow \omega'_S \rightarrow \omega_{aS}$. (b) Polarizations for SIP-CARS. The narrowband field is elliptically polarized with projections onto the x- and y-axes E_{n_x} and E_{n_y}, respectively. The broadband field, E_b is linearly polarized along the x-axis. Detection is performed along $\mathbf{s}_+$ and $\mathbf{s}_-$. E_n is shown as the input to a $\lambda/4$ plate (orientated at angle ϕ to the fast axis) to generate the desired elliptical polarization (direction of propagation is out of the page). (c) The SIP-CARS spectrum of toluene, obtained from the difference between CARS spectra measured along $\mathbf{s}_+$ and $\mathbf{s}_-$, removes the spectral distortion of peaks and the NRB, with peaks now occurring at the correct Raman shifts.

et al. (2014):

$$P_i(\omega_{aS}) = \int d\omega_{pr} \chi_{ijkl}(\omega_{aS} - \omega_{pr}) E_{pr_j}(\omega_{pr}) \times \left[\int d\omega_S E^*_{S_l}(\omega_S) E_{p_k}(\omega_{aS} + \omega_S - \omega_{pr}) \right] \quad (5)$$

where the term inside the square brackets is a cross-correlation of the Stokes and pump fields. The polarization response, and hence the anti-Stokes field, is then given by a convolution with the probe field of the frequency distribution of the excited vibrational modes, determined by the third order susceptibility. The spectral form of the narrowband field can be approximated as $E_n(\omega) = \varepsilon_n \delta(\omega - \omega_n)$, and that of the broadband field defined to be $E_b(\omega) = \varepsilon_b g(\omega)$. As we are only concerned here with spectrally resolved signals the probe field E_{pr} is always narrowband, and noting that $E_{b_y} = 0$ (as defined in Fig. 1(b)), Eqn (5) can then be reduced to two forms, depending on whether (A) $E_p = E_n$ or (B) $E_p = E_b$:

$$P_i(\omega_{aS}) = \chi_{ijk1}(\omega_{aS} - \omega_n) \varepsilon^{A,B}_{jk}(\omega_{aS}, \omega_n) \quad (6)$$

where, for $E_p = E_n$,

$$\varepsilon^A_{jk} = \varepsilon_{n_j} \varepsilon_{n_k} \varepsilon^*_b g(\omega_n - (\omega_{aS} - \omega_n)) \quad (7)$$

and for $E_p = E_b$,

$$\begin{aligned} \varepsilon^B_{jk} &= \varepsilon_{n_j} \int E^*_b(\omega_S) E_b(\omega_{aS} + \omega_S - \omega_n) d\omega_S \\ &= \varepsilon_{n_j} |\varepsilon_b|^2 (g \star g)(\omega_{aS} - \omega_n) \delta_{k1} \end{aligned} \quad (8)$$

where $\star$ is the cross-correlation operator and δ is the Kronecker delta function. The components of the elliptically polarized narrowband field are related by $E_{n_y} = i\eta E_{n_x}$ (where $\eta = tan\phi$), such that the induced material polarizations P_x and P_y may be determined from Eqn (6) to be,

$$P_x = \chi_{1111}(\varepsilon_A + \varepsilon_B) - \eta^2 \chi_{1221} \varepsilon_A, \quad (9)$$

$$P_y = i\eta [\chi_{1122}(\varepsilon_A + \varepsilon_B) + \chi_{1212} \varepsilon_A] \quad (10)$$

where we have summed over both pathways A and B and $\varepsilon_{A,B} = \varepsilon^{A,B}_{11}$. Substituting into Eqn (4) and assuming an isotropic medium (such that $\chi_{1111} = \chi_{1212} + \chi_{1122} + \chi_{1221}$ and $\chi_{1212} = \chi_{2121}$) gives for the SIP-CARS spectrum:

$$\begin{aligned} I_{SIPCARS} \propto\ & 2\varepsilon_A \varepsilon^*_A (\eta^3 - \eta) Im\{\chi_{1111} \chi^*_{1221}\} \\ & + 2\varepsilon_B \varepsilon^*_B \eta Im\{\chi_{1111} \chi^*_{1221}\} + cross\text{-}terms, \end{aligned} \quad (11)$$

where the cross-terms are of the form $\varepsilon_A \varepsilon_B^*$ (or complex conjugate). The non-linear response can be separated into resonant (R) and non-resonant (NR) components, $\chi_{ijkl} = \chi_{ijkl}^{NR} + \chi_{ijkl}^{R}$ and, noting that the non-resonant terms are real and possess Kleinman symmetry,[18] we have

$$I_{SIPCARS} \propto \left[2\varepsilon_A \varepsilon_A^* \left(\eta^3 - \eta\right) - \varepsilon_B \varepsilon_B^* \eta\right] \times \chi_{NR} Im\left\{\frac{1}{3}\chi_{1111}^R - \chi_{1221}^R\right\} + cross\text{-}terms. \quad (12)$$

The two excitation terms in Eqns (7) and (8) have different spectral distributions: $\varepsilon_A(\omega)$ has the form of the spectrum of the broadband beam reflected through the pump frequency into the anti-Stokes region, while $\varepsilon_B(\omega)$ is the autocorrelation of the broadband beam shifted such that the peak is at the pump frequency ω_n (and monotonically decreasing to higher and lower wavenumbers). Spectrally separating the narrowband and broadband fields therefore allows the hybrid excitation scheme to efficiently excite the full spectrum, by using the 2-color excitation to generate signal at higher wavenumbers while the 3-color excitation simultaneously generates signal at low wavenumbers.[3] Implemented this way, $\varepsilon_A(\omega)$ and $\varepsilon_B(\omega)$ have minimal spectral overlap and the cross terms go to zero (or are at least only appreciable over a small spectral range which can be set to be between the fingerprint and C-H stretch Raman spectral regions. This region is typically free of resonances in biological samples).

Substituting for $\varepsilon_{A,B}(\omega)$ in Eqn (12), using Eqns (7) and (8), gives

$$I_{SIPCARS} \propto \left[A_{2col} + A_{3col}\right](1 - 3\rho) \times \chi_{NR} Im\left\{\chi_{1111}^R\right\} \quad (13)$$

where

$$A_{2col} = \sin(4\phi)\, I_n^2 I_b \left|g\left(\omega_n - (\omega_{aS} - \omega_n)\right)\right|^2, \quad (14)$$

$$A_{3col} = \sin(2\phi)\, I_n I_b^2 \left|(g \star g)\left(\omega_{aS} - \omega_n\right)\right|^2. \quad (15)$$

Eqn (13) describes hybrid 2- and 3-color SIPCARS: the first term is the 2-color signal (Eqn (2)), while the second term is the 3-color contribution. The 2-color term Eqn (14) is maximized for ellipticities of the narrowband beam corresponding to $\phi = \pm\pi/8$ and $\phi = \pm 3\pi/8$, whereas the 3-color term Eqn (15) is maximized at $\phi = \pm\pi/4$. Residual shot noise from the cancelled real signal components is reduced for ellipticities with a stronger field strength along the y-axis, orthogonal to the broadband beam polarization. This is because the real signal components are stronger along the x-axis, whereas the amplification of the signal via the NRB is given by Eqns (13)-(15). Thus, to optimize signal to noise requires $\phi \sim \pm 3\pi/8$ for the 2-color term, such that $\phi > \pi/4$ for the 3-color term, in which case the 2- and 3-color signals will have opposite sign. Note that, to avoid the cross-terms of Eqn (11), the spectral form of the broadband beam can be set such that there is essentially no spectral overlap between the 2- and 3-color signals, in which case they do not detract from each other. As the $\sin(2\phi)$ term varies more slowly than the $\sin(4\phi)$ term, a satisfactory compromise with large signal for both terms can be found for $\phi \leq 3\pi/8$.

Experiment

Experiments were performed with the apparatus shown in Fig. 2. The narrowband beam was provided by 10% of the output of a Ti:Sapphire laser (Coherent Mira: 785 nm, 2 ps, 76 MHz, $\sim$24 cm^{-1} FWHM), with the remaining output passed through a photonic crystal fibre (NKT Photonics Femtowhite 800) to generate the broadband beam (800-1040 nm). For 3-color excitation, an angle tuned long-pass interference filter (Semrock LP02-1064RU) was used to block the shorter wavelength end of the broadband beam. The narrowband beam polarization was controlled by a combination of linear polarizer and zero-order half- and quarter-waveplates. Beams were combined on a dichroic mirror and focused into the sample by a 1.3NA oil immersion DIC objective lens, where the pump and Stokes beams average powers were each up to 30 mW (beams were attenuated to avoid sample damage as necessary). Samples were prepared between two glass coverslips, sep-

arated by <60 μm. It should be noted that whilst changing the polarization of the narrowband beam, the spatial overlap of the narrowband/broadband beams at the focus had to be readjusted to account for slight deviations in the narrowband beam.

The signal was collected by an identical objective lens, separated from the excitation fields by a shortpass filter, and then dispersed via an imaging spectrometer (Princeton Instruments Isoplane SCT-320) onto a back-illuminated CCD (Andor Ixon 897+, used with conventional amplifier). A Wollaston prism placed after the collection objective separated the two detection polarizations on the CCD. The position of the Wollaston prism before the tube lens, and the optics coupling the microscope to the spectrometer, were chosen such that the prism was imaged onto the grating; in this way, both detected polarizations were able to fill the grating without vignetting. Before entering the spectrometer, the signal was circularly polarized by an achromatic quarter-wave plate to account for the different grating reflectivity for each polarization.

The 3-color signal depends on the spectral amplitude autocorrelation of the broadband beam (Eqn (15)), which increases markedly with the phase coherence of the pulse. It is consequently much higher for transform limited pulses, which must be <25 fs to achieve the required spectral width. The laser system employed (2 ps pulses and broadband excitation generated with a PCF) was therefore not well suited for the generation of strong 3-color signals; however, it was sufficient to demonstrate the proof-of-principle. For 2-color measurements in the fingerprint region the 3-color signal could be suppressed by temporally dispersing the broadband beam, by passing it through 50mm of H-ZF13 glass. Inclusion of this glass block limited the 3-color CARS to below 520 cm^{-1} (determined via the monotonically decreasing 3-color CARS spectrum for water, which is dominated by NRB in the fingerprint region).

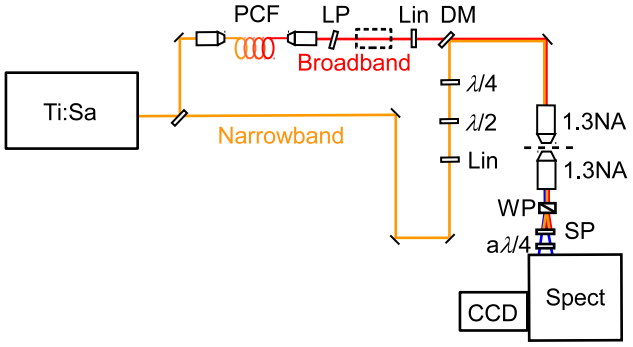

Figure 2: Experimental setup. 10% of the output of a Ti:Sapphire oscillator (76 MHz, 2ps) served as the narrowband beam (785 nm) while the remaining power was input to a photonic crystal fiber (PCF) to generate the broadband (800-1040 nm) pulse. An angle tuned long-pass interference filter (LP) was used to block the shorter wavelength end of the broadband beam for 3-color measurements. Beams were combined on a dichroic mirror (DM) and focused into the sample by a 1.3NA DIC objective lens. Samples were prepared between two coverslips, separated by <60 μm. The signal was collected by an identical objective lens, separated from the excitation fields by a short-pass filter (SP), and then dispersed via grating spectrometer onto a CCD. The pump/probe ellipticity was controlled by a combination of linear polarizer (Lin) and zero-order half- and quarter-waveplates ($\lambda/2$ and $\lambda/4$, respectively). A Wollaston prism (WP) was placed after the collection objective lens to separate the two detection polarizations on the CCD. The beams were again circularly polarized before the spectrometer by an achromatic quarter-wave plate (a$\lambda/4$) to account for the different grating reflectivity for each polarization. For 2-color measurements in the fingerprint region a 50 mm glass block was inserted in the broadband beam (dashed line).

Results

The 2-color SIP-CARS spectrum of the fingerprint region of cyclohexane (obtained with the 50mm thick glass block present) is shown in Fig. 3(b), for comparison with the 3-color measurements below. The measured sum spectrum of water in the fingerprint region (Fig.

3(a)), which accounted for the spectral variation of the broadband beam and the instrument response, was used to normalize the SIP-CARS spectra. As expected, the SIP-CARS spectrum contains both positive and negative peaks, determined by the polarization ratio ρ of each mode, and corresponds to a linear combination of polarized Raman spectra, Eqn (3), with symmetric, unshifted spectral lines as we have shown previously.[9] For the polarized (p) modes at 801 cm^{-1} and 1157 cm^{-1}, $\rho = 0.04$ and 0.22 respectively,[19] such that the symmetry prefactor term $(1 - 3\rho)$ in Eqns (2) and (13) is positive. In contrast, $\rho = 0.75$, and hence $(1 - 3\rho)$ is negative, for the depolarized (dp) modes at 1027 cm^{-1}, 1266 cm^{-1} and 1346 cm^{-1};[19,20] experimentally, these modes are observed to have the opposite sign to the two polarized modes in the SIP-CARS spectrum.

For the 3-color SIP-CARS spectrum, shown in Fig. 3(d), the long-pass filter was angle-tuned such that the broadband beam was blocked below 923 nm, corresponding to 2-color CARS above 1900 cm^{-1}. The spectrum of water over the fingerprint region was therefore determined by the autocorrelation of the broadband beam, modulated by the detection system response. The sum spectrum of water in the fingerprint region was used to normalize the SIP-CARS spectra. The cyclohexane peaks can clearly be seen, though inverted with respect to the 2-color spectrum.

By putting a higher angle-of-incidence on the long-pass filter it was possible to extend the 2-color region of the spectrum to lower wavenumbers. Fig. 4(a) shows a hybrid 2/3-color spectrum of cyclohexane, with 3-color SIP-CARS below 1300 cm^{-1} and the 2-color process dominating above. Around 1300 cm^{-1}, at the cut-on point of the filter, cross-terms of Eqn (12) are expected to be of similar magnitude to Eqn (13), but away from the transition region either term of Eqn (13) will be dominant. Note that the peak in the 2-color region at 1444 cm^{-1} is reversed with respect to the peaks in the 3-color region, as expected from Eqn (13).

Eqns (14)-(15) predict the behaviour of the signal to vary differently in the 2-color/3-color regions with changes in either the power of the laser beams or the polarization state of the narrowband beam. For laser power, the signal is expected to be linearly dependent on the narrowband beam in the 3-color region and quadratically dependent on it in the 2-color region, and *vice versa* for the broadband beam. Fig. 4(c) and Fig. 4(d) confirm that this holds true experimentally. For the polarization state of the narrowband beam, we expect the 3-color region to vary as $\sin(2\phi)$ and the 2-color region to vary as $\sin(4\phi)$, with $\phi = 0, \pi/2$ corresponding to linear polarization and $\phi = \pi/4$ corresponding to circular polarization. Fig. 4(b) shows, again, good agreement with the theoretical predictions.

Conclusions

The use of intrapulse 3-color excitation enables, in conjunction with interpulse 2-color excitation, broadband CARS spectroscopy (and hence hyperspectral imaging) across a broad Raman spectral range with high sensitivity and spectral resolution.[3] We demonstrate the applicability to simultaneous 2-color and 3-color excitation of SIP-CARS, which enables broadband CARS spectroscopy with full removal of non-resonant background using only passive polarization optics.[9] SIP-CARS spectra are directly related to polarized Raman difference spectra, with intrinsic signal amplification by the non-resonant response and additional information on molecular symmetry through the sign of SIP-CARS peaks (determined by the Raman depolarization ratio). Although the polarization configuration required to deliver maximum signal strength are different for 2-color and 3-color excitation, a good compromise is achievable with a strong signal resulting from both excitation paths, and with a reversal of sign of the measured polarized Raman difference signal. In conclusion, the application in SIP-CARS of an ultrafast laser source for transform-limited broadband excitation, provides the potential for fast, all-optical quantitative hyperspectral Raman imaging over the entire biologically relevant Raman window.

Acknowledgement PS acknowledges sup-

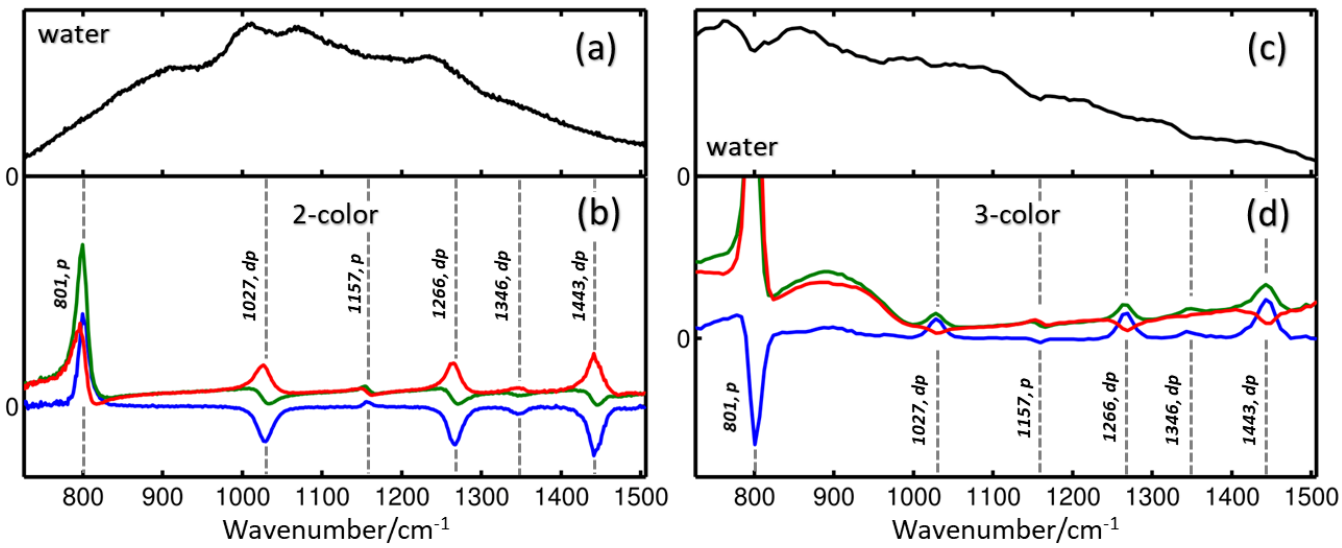

Figure 3: (a, b) 2-color SIP-CARS, with inclusion of a 50mm glass block in the broadband beam, to suppress 3-color CARS. (c, d) 3-color SIP-CARS; the broadband beam is blocked below 932 nm by a long-pass filter, such that 2-color CARS can only occur above 1900 cm^{-1}. (a, c) The sum spectrum ($S_+ + S_-$) of water; in (a) this is essentially NRB of water arising from 2-color CARS, modulated by the Stokes spectrum and detection system response, while in (c) this results from the NRB of water excited by the autocorrelation of the Stokes spectrum and modulated by detection system response. (b) 2-color spectrum of cyclohexane (normalized by the spectrum (a)). (d) 3-color spectrum of cyclohexane (normalized by the spectrum (c)); Peaks are inverted with respect to the 2-color spectrum in (b). (b, d) The peaks have their known wavenumbers assigned and labelled according to whether they are polarized (p, $0 < \rho < 0.75$) or depolarized (dp, $\rho = 0.75$).[19,21] Green: $\mathbf{S}_+$ spectrum; Red: $\mathbf{S}_-$ spectrum; Blue: SIP-CARS ($\mathbf{S}_+ - \mathbf{S}_-$) spectrum.

port from an EPSRC studentship. We are grateful for support from the Royal Society's Paul Instrument Fund.

References

(1) Day, J. P. R.; Domke, K. F.; Rago, G.; Kano, H.; Hamaguchi, H.-o.; Vartiainen, E. M.; Bonn, M. *The Journal of Physical Chemistry B* **2011**, *115*, 7713–7725.

(2) Polli, D.; Kumar, V.; Valensise, C. M.; Marangoni, M.; Cerullo, G. *Laser & Photonics Reviews* **2018**, *12*, 1800020.

(3) Camp, C. H.; Lee, Y. J.; Heddleston, J. M.; Hartshorn, C. M.; Hight Walker, A. R.; Rich, J. N.; Lathia, J. D.; Cicerone, M. T.; Cicerone, M. T. *Nature Photonics* **2014**, *8*, 627–634.

(4) Fu, D.; Lu, F.-K.; Zhang, X.; Freudiger, C.; Pernik, D. R.; Holtom, G.; Xie, X. S. *Journal of the American Chemical Society* **2012**, *134*, 3623–3626.

(5) Ozeki, Y.; Umemura, W.; Otsuka, Y.; Satoh, S.; Hashimoto, H.; Sumimura, K.; Nishizawa, N.; Fukui, K.; Itoh, K. *Nature Photonics* **2012**, *6*, 845–851.

(6) Wang, P.; Liu, B.; Zhang, D.; Belew, M. Y.; Tissenbaum, H. A.; Cheng, J.-X. *Angewandte Chemie International Edition* **2014**, *53*, 11787–11792.

(7) Freudiger, C. W.; Yang, W.; Holtom, G. R.; Peyghambarian, N.; Xie, X. S.; Kieu, K. Q. *Nature Photonics* **2014**, *8*, 153–159.

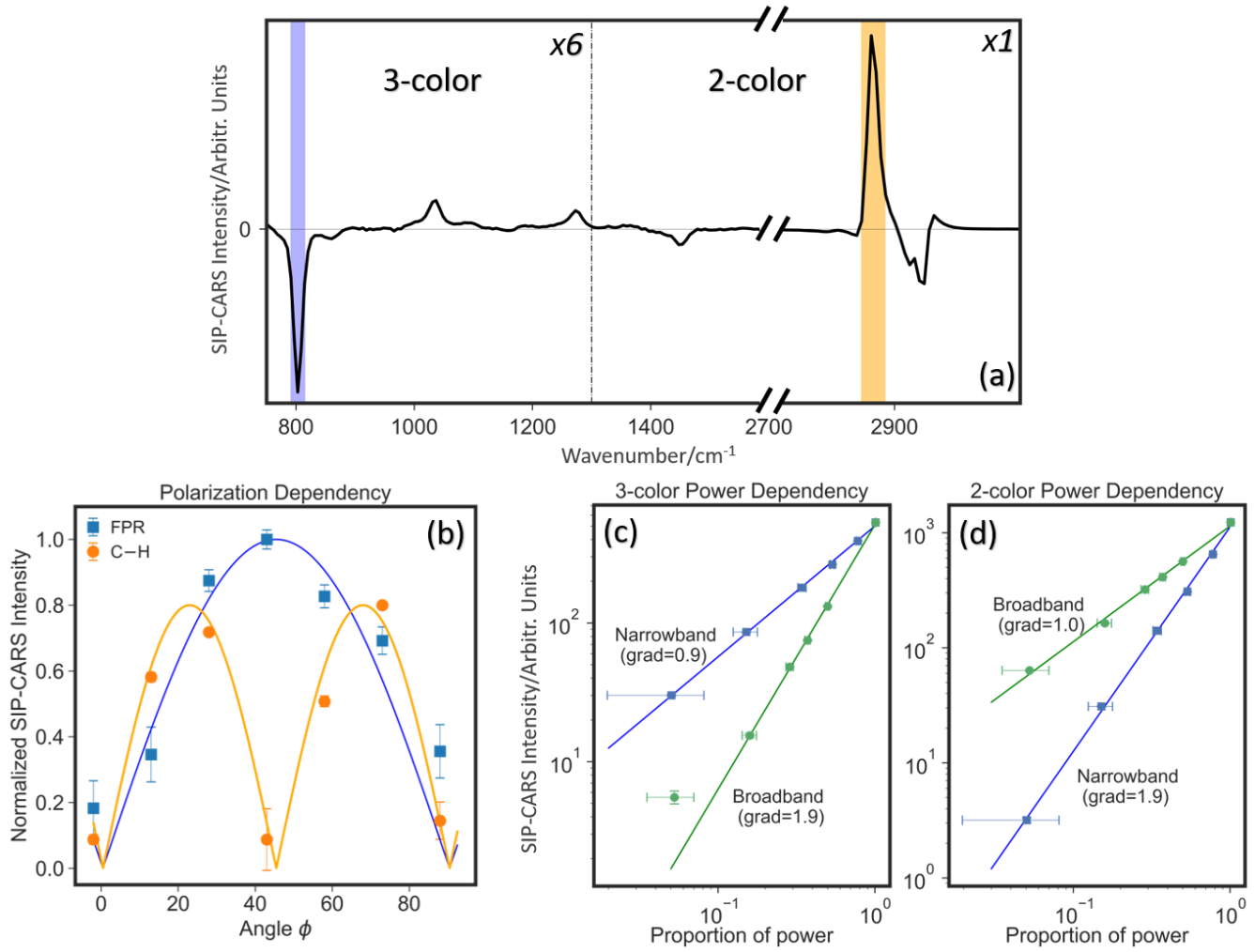

Figure 4: (a) Hybrid 2-color/3-color SIP-CARS spectrum of cyclohexane, spectral acquisition time of 50 ms. The long-pass filter in the broadband beam is angle-tuned to block wavelengths below 874 nm, corresponding to 2-color CARS above 1300 cm^{-1} (dashed line in (a)) and 3-color CARS below. The fingerprint region has been magnified for comparative purposes. (b) Polarization dependency of the 2-color/3-color excitation mechanisms. The plot shows the variation in intensity for the 801.3 cm^{-1} peak in the fingerprint region (FPR) fitted with a $|\sin(2\phi)|$ curve and the variation in intensity for the 2852.9 cm^{-1} peak in the C-H region fitted with a $|\sin(4\phi)|$ curve. (c, d) Power dependency of the 2-color/3-color excitation mechanisms. Using the same two peaks as in (b), the plots show that the narrowband and broadband vary linearly and quadratically, respectively, in the 3-color region and *vice versa* in the 2-color region. Both the polarization dependency measurements and the power dependency measurements are in good agreement with the theoretical predictions from Eqns (14)-(15).

(8) Camp, C. H.; Lee, Y. J.; Cicerone, M. T. *Journal of Raman Spectroscopy* **2016**, *47*, 408–415.

(9) Littleton, B.; Kavanagh, T.; Festy, F.; Richards, D. *Physical Review Letters* **2013**, *111*, 103902.

(10) Dudovich, N.; Oron, D.; Silberberg, Y. *Nature* **2002**, *418*, 512–514.

(11) Vartiainen, E. M.; Rinia, H. A.; Müller, M.; Bonn, M. *Optics Express* **2006**, *14*, 3622.

(12) Liu, Y.; Lee, Y. J.; Cicerone, M. T. *Journal of Raman Spectroscopy* **2009**, *40*, 726–731.

(13) Cicerone, M. T.; Aamer, K. A.; Lee, Y. J.; Vartiainen, E. *Journal of Raman Spectroscopy* **2012**, *43*, 637–643.

(14) Masia, F.; Glen, A.; Stephens, P.; Borri, P.; Langbein, W. *Analytical Chemistry* **2013**, *85*, 10820–10828.

(15) Eesley, G. L. *Coherent Raman spectroscopy*; p 142.

(16) Lim, S.-H.; Caster, A. G.; Leone, S. R. *Physical Review A* **2005**, *72*, 041803.

(17) Langbein, W.; Rocha-Mendoza, I.; Borri, P. *Applied Physics Letters* **2009**, *95*, 081109.

(18) Kleinman, D. A. *Physical Review* **1962**, *126*, 1977–1979.

(19) Toleutaev, B. N.; Tahara, T.; Hamaguchi, H. *Applied Physics B Laser and Optics* **1994**, *59*, 369–375.

(20) Saito, Y.; Ishibashi, T.; Hamaguchi, H. *Journal of Raman Spectroscopy* **2000**, *31*, 725–730.

(21) Shimanouchi, T. *Journal of Physical and Chemical Reference Data* **1977**, *6*, 993–1102.